Article:

Antonelli, L. orcid.org/0000-0003-0694-948X, Barbato, F., Mancelli, D. et al. (14 more authors) (2019) X-ray phase-contrast imaging for laser-induced shock waves. EPL. 35002. ISSN 1286-4854

https://doi.org/10.1209/0295-5075/125/35002

epl draft

X-ray phase-contrast imaging for laser-induced shock waves

L. Antonelli[1,2], F. Barbato[3], D. Mancelli[4,5], J. Trela[4], G. Zeraouli[6,7], G. Boutoux[4], P Neumayer[8], S. Atzeni[1], A. Schiavi[1], L. Volpe[6,7], V. Bagnoud[8], C. Brabetz[8], B. Zielbauer[8], P. Bradford[2], N. Woolsey[2], B. Borm[9] and D. Batani[4]

[1] *Dipartimento SBAI, Università degli Studi di Roma "La Sapienza", Via Antonio Scarpa 14, 00161, Roma, Italy*
[2] *York Plasma Institute, Department of Physics, University of York, York, YO10 5DQ, United Kingdom*
[3] *Empa - Swiss Federal Laboratories for Materials Science and Technology, Überlandstrasse 129, CH8600 Dübendorf, Switzerland*
[4] *Université de Bordeaux, CNRS, CEA, CELIA (Centre Lasers Intenses et Applications), UMR 5107, F-33405 Talence, France*
[5] *University of the Basque Country (UPV/EHU), Donostia International Physics Center (DIPC), Donostia/San Sebastin, Basque Country, Spain*
[6] *CLPU, Centro de Láseres Pulsados, Edificio M5. Parque Científico. C/ Adaja, 8. 37185 Villamayor, Salamanca, Spain*
[7] *Universidad de Salamanca Facultad de Ciencias. Plaza de los Caídos, s/n. 37008 Salamanca, Spain*
[8] *GSI Helmholtzzentrum für Schwerionenforschung GmbH, Planckstraße 1, 64291 Darmstadt, Germany*
[9] *Goethe-Universität Frankfurt, Max-von-Laue-Straße 1, 60438 Frankfurt am Main, Germany*

PACS `52.50.Lp` – Heating plasma by shock-wave
PACS `52.38.Mf` – Laser ablation laser-plasma interactions
PACS `87.59.-e` – X-ray imaging

Abstract – X-ray phase-contrast imaging (XPCI) is a versatile technique with applications in many fields, including fundamental physics, biology and medicine. Where X-ray absorption radiography requires high density ratios for effective imaging, the image contrast for XPCI is a function of the density gradient. In this letter, we apply XPCI to the study of laser-driven shock waves. Our experiment was conducted at the Petawatt High-Energy Laser for Heavy Ion EXperiments (PHELIX) at GSI. Two laser beams were used: one to launch a shock wave and the other to generate an X-ray source for phase-contrast imaging. Our results suggest that this technique is suitable for the study of warm dense matter (WDM), inertial confinement fusion (ICF) and laboratory astrophysics.

X-ray phase contrast imaging (XPCI) is based on the phase-shift of X-ray photons induced by a density gradient. In the presence of a density variation, the incident X-ray photons are deflected from higher density to lower density regions, generating an intensity fringe at the gradient. Synchrotrons and Free Electron Lasers are ideal experimental platforms for XPCI because they can deliver coherent radiation at high energy (to accentuate the phase-shift and limit photon absorption) and high flux [1–3]. It is also possible to use broadband incoherent radiation for phase contrast imaging, however the corresponding X-ray source must be very small. One method for generating small-scale X-ray sources suitable for XPCI is to use laser-irradiated solid targets [4,5]. XPCI has already made an important contribution to the fields of biology and medicine [6–9], but laser-driven XPCI could also be applied to studies of warm dense matter (WDM), laboratory astrophysics and inertial confinement fusion (ICF). The sensitivity of XPCI to density gradients means it can probe a range of different densities in the same measurement. This is useful for studying hydrodynamic processes at material interfaces, such as the Richtmyer - Meshkov and Kelvin - Helmholtz instabilities. What is more, since laser-driven XPCI uses a high-energy probe, it is also possible to study radiative phenomena relevant to astrophysics. Large-scale laser facilities such as the National Ignition Facility (NIF) [10] and Laser Mégajoule (LMJ) [11] enable us to study matter in extreme conditions and both have dedicated beam-

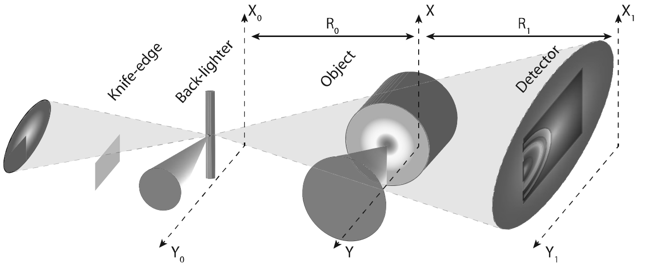

Fig. 1: Experimental set-up showing the short-pulse back-lighter and long-pulse drive beams.

lines for target probing: the Advanced Radiographic Capability (ARC) [12] and the PETawatt Aquitaine Laser (PETAL) [13]. With the increased precision and detail available through XPCI, the development of XPCI lines on these facilities could open up new possibilities in diagnostic imaging. Though laser-driven X-ray absorption radiography has been successfully demonstrated on many experiments (some examples are reported in [14–20]), XPCI using laser-produced X-ray sources has been less intensively studied. A significant advance in the application of laser-driven bremsstrahlung X-ray sources to XPCI was shown by Workman et al. in 2010 [21], however the quality of the images they obtained did not allow for a comprehensive study of shock wave characteristics. In [22], a numerical study of cryogenic beryllium capsules using phase-contrast imaging is presented, however a proof-of-principle laser experiment is necessary to pin down the requirements of a single-shot, laser-produced X-ray source for XPCI. In this letter we present the results of an experiment at the PHELIX facility [23] where XPCI was used to study a laser-induced shock-wave. The total energy delivered by the laser was 50 J, divided equally between the short pulse beam (to generate the X-ray source) and the long pulse beam (to drive the shock wave). The experimental layout can be seen in Figure 1.

A 25 J, 0.5 ps, 1.06 μm wavelength laser pulse was focussed onto a tungsten wire with a 5 μm focal spot, leading to on-target intensities of around 6×10^{19} Wcm^{-2}. Under these conditions, a large portion ($\sim 10-20\%$) of the incident laser energy is transferred to relativistic electrons [24] that propagate through the wire and emit bremsstrahlung radiation. These hot electrons were monitored using a bremsstrahlung cannon and highly oriented pyrolytic graphite (HOPG) crystal spectrometer. A knife edge was used to characterize the source dimensions on each shot. In the horizontal direction, the source was measured to be 5 μm across (the same as the wire diameter), while the size measured along the wire was 30 μm. The characteristics of our X-ray source are consistent with phase-contrast enhancement. If we assume Fresnel diffraction, the recorded pattern on the detector surface results from the superposition of waves coming from a coherence area commensurate with the transversal coherence length, l_t, which is the minimum distance between two points in the transverse direction with a correlated phase, defined as:

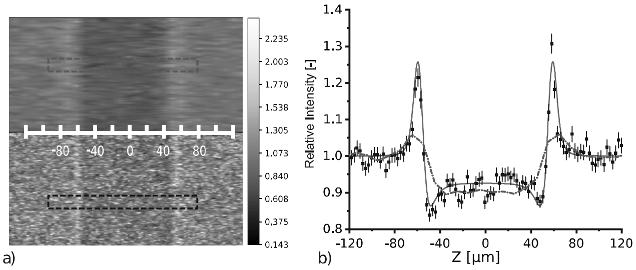

Fig. 2: a) XPCI image of plastic wires. The upper part corresponds to the IP detector while the lower part corresponds to the CCD. b) X-ray transmission profile from experimental CCD image (black dots) and synthetic profile (red line). The blue dot-dashed line is the corresponding layout on the IP from the upper part of the image (dashed blue line).

$$l_t \approx \frac{R_0 \lambda}{s} \tag{1}$$

where R_0 is the distance from source to sample, s is the source size (in our case l_t has a different value in the vertical and horizontal directions due to the source geometry) and λ is the X-ray wavelength. In other words, l_t has to be larger than the scale length for the structure to be resolved. In the case of a laser-induced shock wave, l_t should be of the order of a few microns. Equation 1 gives a criterion to evaluate a source for XPCI which is more restricted than reality [25]. Taking the source dimensions into account, the X-ray wavelength ranged from 1.2 to 2.0 Å, and the distance R_0 was 24.5 cm, the minimum value of l_t is 1 μm in the vertical direction and its maximum is 10 μm in the horizontal direction (where the source size is limited to 5 μm).

A 25 J, 2 ns, 1.06 μm wavelength laser pulse was used to launch a shock wave in a plastic (C_8H_8) cylinder with a diameter of 300 μm. With a focal spot diameter of 50 μm, the intensity was about 3×10^{14} W/cm^2. We used two different detectors to record our images: an Image Plate (IP) and Andor CCD camera. To remove any contribution coming from the interaction of the long pulse with the target, a 500 μm-thick Polymethyl methacrylate (PMMA) window and a 40 μm thick Al filter were placed in front of our detectors. The transmission of these filters ranged from 2% at 5 keV to 63% at 10 keV.

We tested our set-up by imaging cylindrical nylon wires with diameters from 120 to 400 μm. The results are shown in Figure 2. The image shows the presence of phase contrast at the edges of the wire and low levels of absorption (around 10% of the incident X-ray radiation below 5 keV). If we consider the transverse profile of one of the wire with respect to the wire axis (represented by black dots in Figure 2b), the phase contrast edges are clearly visible while absorption plays a minor role. The red line in Figure 2b is the synthetic profile calculated using our own code. The code was designed to calculate X-ray absorption and phase contrast, taking into account the X-ray spectrum, source size and spatial intensity distribution and solving the Kirchoff-Fresnel equation using the Fresnel approximation [26]. The code works in cylindrical geometry and it takes into account the source spectra, source size and detector resolution in a similar way as described in [27,28]. Moreover, the density map associate to the object has to be provided. We used the mass absorption coefficient for cold Nylon available in the NIST database [29]. Considering the experimental limitations (detector resolution, low photon flux, etc.) there is good agreement between experiment and simulation. The blue dot-dashed lines correspond to a layout of the same wire on the IP. Some of the details are lost due to the lower resolution, as evinced by the lower ratio between the diffraction peak maximum and source intensity. The amplitude of the error bars is calculated from analysis of fluctuations in source intensity.

In Figure 3a, we observe a laser-driven shock wave propagating inside a plastic cylinder. This image was taken 8 ns after the end of the driving pulse using IP as detector. There is evidence of both absorption and phase-contrast processes, with the strongest phase-contrast at the target-vacuum edge (P3) and inside the shocked region (P2). It is also present on the shock wave front (compressed-uncompressed interface, P1). XPCI is sensitive to density variations and can provide information on shock wave propagation even at moderate laser intensity. The X-ray intensity inside the shock wave is higher than the vacuum background intensity, suggesting that a strong density gradient is present in the low-density region before the shock front (P2). To model this internal structure, we ran a number of simulations using the hydrodynamic code DUED [30] coupled to the bespoke XPCI simulation code. As for the nylon wires, we again assumed cold opacity for the Polystyrene. Indeed, the 5 - 10 keV backlighter photons are mainly absorbed by the K-shell electrons in the carbon atoms if they are not fully ionized. The typical temperature of shock target at this intensity is few eV, with a low degree of ionization. In such case the use of cold opacity leads to an error no more than 1% [31]. The synthetic radiograph is remapped in a lower resolution image to match the experimental resolution. Initially, we assumed a super-Gaussian focal intensity distribution with a diameter of 50 μm, a square time shape with a pulse duration of 2 ns and an energy of 25 J (corresponding to the nominal parameters of the laser). Numerical noise calculated from the experimental measurement was added to simulation. The experimental noise is measured directly on the experimental data where the target is not present. Intensity oscillation follows a Gaussian behaviour with a FWHM equal to 10%. A deviation from the simulated intensity following such a behaviour is then added to the synthetic radiograph. The results are shown in Figure 3b. Although reducing the energy in the simulation allowed us to match the position of the wavefront on-axis, the synthetic image looks quite different from the experimental data. Moreover the phase contrast at the simulated shock front is higher than in the experiment, which implies that these simulations have unrealistically steep density gradients. Figure 4a shows the intensity profile along the horizontal axis (to help reduce noise, the central line was averaged with the two nearest points in the transverse direction). The numerical profiles were taken without numerical noise. In this case we introduced the error bar on the experimental data. Our code reproduces the peak corresponding to the vacuum-target interface and also the position of the shock front. The peak intensity is different, however, and we can deduce that the simulation is predicting a higher density-ratio between the shocked and unshocked regions since the width of the simulated and experimental peaks is comparable. Though significant phase-contrast is visible inside the simulated shock, the structure is not well-reproduced. Instead of a single, intense peak, the red profile has a weaker, bimodal structure. In addition, the bright region is much more extended in the simulation than the experiment. One explanation for the discrepancy comes directly from the experimental image: A localized bright region inside the shock wave is indicative of a strong density gradient which would "deflect" photons from the higher density region to the lower one. This single intensity peak is probably due to the rarefaction wave which stands behind the shock front and inside the shocked material. Moreover the strong 2D evolution observed is more consistent with a smaller focal spot. We could not characterize the focal spot at full power and there was no phase plate to smooth the focal spot distribution. It is therefore reasonable to expect high intensity spikes which would affect laser energy deposition. In addition, considering the wavelength used, we were also more susceptible to parametric effects which could modify the energy absorption.

To test this hypothesis, we performed several simulations where we progressively reduced the laser spot size from 50 μm down to a 5 μm central spike. Results for the smallest focal spot are detailed in Figure 3c. Here, we can distinguish a bright region corresponding to a single phase-contrast peak that is broadly consistent with our experimental results. While the agreement is not perfect, this simulation proves that a spike in laser intensity can dramatically affect the resulting phase-contrast image. The laser energy was kept at 25 J in these simulations. In Figure 4b, we present on-axis intensity profiles for the experiment alongside numerical simulations with a smaller focal spot. A single, intense peak is apparent in the central region that is qualitatively consistent with the experiment. One explanation for a smaller focal spot in our experiment could be self-focusing of the laser beam [32,33]. The laser pulse duration was long (τ = 2 ns), which would allow the laser to interact with plasma generated earlier in the interaction. In order to improve the agreement, a more detailed characterization of the focusing condition is required. Moreover, the experimental image 3a shows a non uniform curvature radius of the shock front. This suggest that we should treat this as a three dimensional problem,

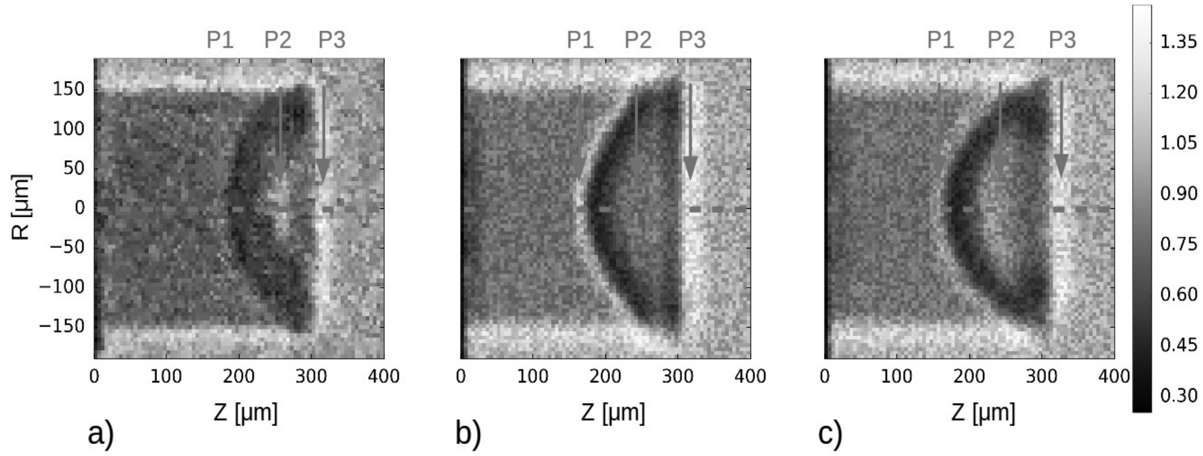

Fig. 3: Comparison between a) XPCI from the experiment, b) A synthetic XPCI image calculated using a specific module coupled to the DUED hydrodynamic code using the nominal focal spot and c) The synthetic XPCI image, using a small focal spot. A numerical noise was added to the images b) and c) according to the experimental measurement.

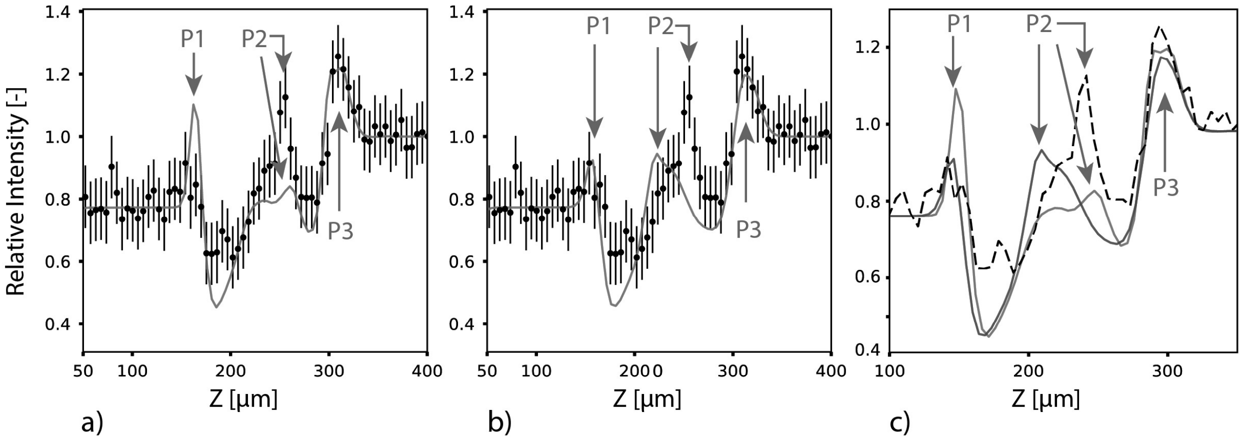

Fig. 4: Comparison between the profile along the propagation axis of a) XPCI simulation with nominal focal spot dimension, b) reduced focal spot dimension. Image c) shows the profile comparison between the simulations (red and blue lines) with the experiment (black dashed line).

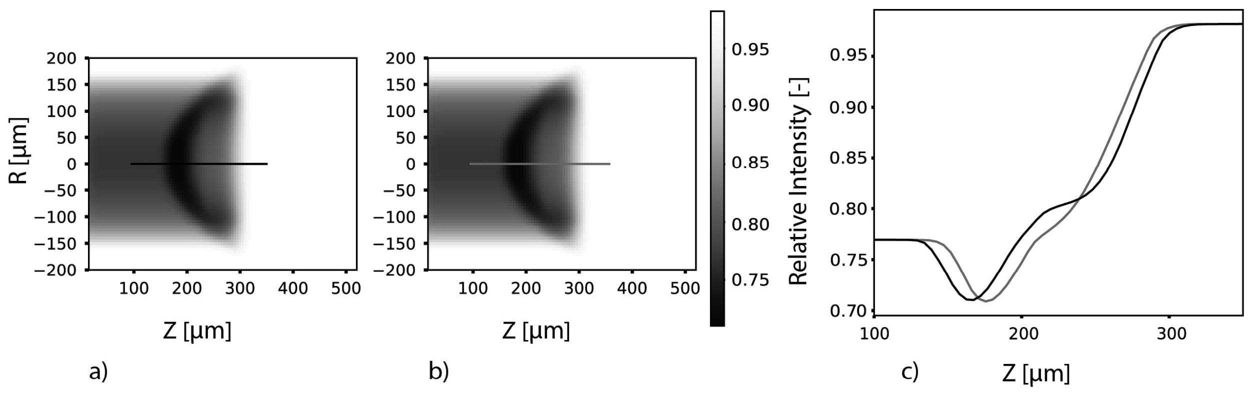

Fig. 5: Synthetic radiographs corresponding to the simulation with a) nominal focal spot and b) reduced focal spot. The image c) compares the intensity profiles along the axis of the image a) (black line) and b) (red line).

using a 3D code with a detailed knowledge of the energy distribution inside the focal spot. However the high quality XPCI images allow a detailed study of the shock shape. By contrast, X-ray absorption radiography does not provide us with the same level of detail. To prove this, we can compare the synthetic absorption radiography of the two simulations. The results are shown in Figure 5a and 5b. It is much harder to identify differences between the simulations using X-ray absorption than with phase contrast imaging (cf. Figure 3b and 3c). In Figure 4c, we show on-axis intensity profiles for the images in Figure 3b and 3c. The red and black absorption profiles are similar, but the red is slightly shifted with the suggestion of a central bump. The energy deposition is different in the two cases and this can cause a difference in the shock velocity. In the case of a small focal spot (red), the 2D effects are stronger and they cause energy to diffuse transverse to the propagation axis. Figure 4 shows the same profile with the phase contrast included. Even accounting for the low resolution of the detector (IP), the structure of the shock wave and the rarefaction wave have been successfully observed. Experimental work has already been done to compare absorption radiography and XPCI in other contexts. In [28], for example, X-ray imaging of a locust demonstrates that XPCI is able to detect features that are completely absent from images made using absorption radiography. The superior sensitivity of XPCI could open up new avenues in the study of warm dense matter, laboratory astrophysics or hydrodynamic instabilities at a variety of densities.

In this work we have presented new XPCI data from the PHELIX laser system at GSI in Germany, using a broadband X-ray source generated by a single laser beam. Our set-up was first tested on static objects and then used to image a laser-driven shock wave. In both cases, phase-contrast at the density interfaces could be clearly discerned. The intrinsic sensitivity of XPCI to density gradients enabled us to observe subtle details in the structure of the shock wave even at low X-ray flux (only 25 J in the backlighter). At larger facilities, where more energetic backlighter beams produce higher X-ray fluxes, the quality of the data would be significantly improved (the signal-to-noise ratio would increase). XPCI is more sensitive to density gradients than X-ray absorption radiography and works well with polychromatic sources. This experiment proved that XPCI can be a useful tool in studies of warm dense matter and high energy density physics, paving the way for testing on large-scale laser facilities.

* * *

This work has been carried out within the framework of the EUROfusion Enabling Research Project: AWP17-ENR-IFE-CEA-01 ”Preparation and Realization of European Shock Ignition Experiments” and has received funding from the Euratom research and training programme 2014-2018 under grant agreement No 633053. The views and opinions expressed herein do not necessarily reflect those of the European Commission. The research leading to these results has received funding from LASERLAB-EUROPE (grant agreement no. 654148, European Union’s Horizon 2020 research and innovation programme). The authors thanks Dr D Bleiner for having contributed to the purchase of a few targets used in the experiment described in this paper.

REFERENCES

[1] Schropp A., et al., *Scientific reports*, **5** (2015) 11089.

[2] Hawreliak J., Erskine D., Schropp A., Galtier E.C., and Heimann P., *AIP Conference Proceedings*, **1793** (2017) 090006.

[3] Nagler B., et al., *Journal of synchrotron radiation*, **22** (2015) 520-5.

[4] Fourmaux S., et al., *Optics letters*, **36** (2011) 2426-8.

[5] Kneip s., et al., *Applied Physics Letters*, **99** (2011) 093701.

[6] Davis T.J., Gao D., Gureyev T.E., Stevenson A.W., and Wilkins S.W., *Nature*, **373** (1995) 11089.

[7] Snigirev A., Snigireva I., Kohn V., Kuznetsov S., and Schelokov I., *Review of scientific instruments*, **66** (1995) 5486-92.

[8] Momose A., Takeda T., Itai Y., and Hirano K., *Nature medicine*, **2** (1996) 473-5.

[9] Wilkins S.W., Gureyev T.E., Gao D., Pogany A., and Stevenson A.W., *Nature*, **384** (1996) 335.

[10] Miller G.H., Moses E.I., and Wuest C.R., *Optical Engineering*, **43** (2004) 2841-54.

[11] Fleurot N., Cavailler C., and Bourgade J.L., *Fusion Engineering and Design*, **74** (2005) 147-54.

[12] Fleurot N., Cavailler C., and Bourgade J.L., *Journal of Physics: Conference Series*, **244** (2010) 032003.

[13] Batani D., Hulin S., Ducret J.E., and dHumieres E., *Acta Polytechnica*, **53** (2013) 37.

[14] Benuzzi-Mounaix A, et al., *Plasma physics and controlled fusion*, **48** (2006) B347.

[15] Le Pape S, et al., *Review of Scientific Instruments*, **79** (2008) 106104.

[16] Antonelli, et al., *Physical Review E*, **95** (2017) 063205.

[17] Antonelli, et al., *Journal of Instrumentation*, **79** (2018) C01013.

[18] Kritcher A.L., et al., *High Energy Density Physics*, **10** (2014) 27-34.

[19] Del Sorbo D., et al., *Laser and Particle Beams*, **33** (2015) 525-34.

[20] Morace A., et al., *Physics of Plasmas*, **21** (2014) 102712.

[21] Workman J., Cobble J., Flippo K., Gautier D.C., Montgomery D.S., and Offermann D.T., *Review of scientific instruments*, **21** (2010) 10E520.

[22] Montgomery D.S., Nobile A., and Walsh P.J., *Review of scientific instruments*, **75** (2004) 3986-8.

[23] Neumayer P., et al., *Laser and Particle Beams*, **23** (2005) 385-9.

[24] Schönlein A., et al., *EPL (Europhysics Letters)*, **114** (2016) 45002.

[25] Wu X., and Liu H., *Medical physics*, **30** (2003) 2169-79.

[26] Cowley J.M., *Diffraction physics*, edited by Elsevier, Vol. **9** 1995, p. 481.

[27] Olivo A., and Speller R., *Physics in Medicine & Biology*, **51** (2006) 3015.

[28] Arfelli F., et al., *Physics in Medicine & Biology*, **43** (1998) 2845.

[29] J. H. Hubbell and S. M. Seltzer, *National Institute of Standards and Technology*, **Report No. NISTIR 5632** (1995) (unpublished).

[30] Atzeni S., et al., *Computer physics communications*, **169** (2005) 153-9.

[31] Fujioka S., et al., *hysics of Plasmas*, **10** (2003) 4784-89.

[32] Young P.E., Hammer J.H., Wilks S.C., and Kruer W.L., *Physics of Plasmas*, **2** (1995) 2825-34.

[33] Young P.E., Baldis H.A., Drake R.P., Campbell E.M., Estabrook K.G., *Physical review letters*, **61** (1988) 2336.